catalysts

MDPI

Article

Optimizing the Incorporation Modes of TiO_2 in TiO_2-Al_2O_3 Composites for Enhancing Hydrodesulfurization Performance of Corresponding NiMoP-Supported Catalysts

Ranran Hou, Qinghe Yang, Shuangqin Zeng, Jun Bao, Hong Nie *, Chuangchuang Yang, Yanzi Jia, Anpeng Hu and Qiaoling Dai

SINOPEC Research Institute of Petroleum Processing Co., Ltd., 18 Xue Yuan Road, Beijing 100083, China
* Correspondence: niehong.ripp@sinopec.com; Tel.: +86-108-236-8928

Abstract: TiO_2-Al_2O_3 supports with different incorporation methods of titania were synthesized via three methods: impregnation (TA-I), co-precipitation (TA-CP), and co-precipitation–hydrothermal treatment (TA-HT). And the NiMoP catalysts prepared on the corresponding supports were evaluated for hydrodesulfurization (HDS) reactions. The results demonstrated that the Ti atoms in TA-I are attached to alumina through hydroxyl groups, while the Ti atoms in TA-CP and TA-HT can be dispersed in the alumina skeleton. Variations in the incorporation modes of TiO_2 affect the support properties, consequently influencing the nature of the active metal on the supports. The Ti atoms dispersed in the Al_2O_3 skeleton allow an increase in the basic hydroxyl groups. Meanwhile, TiO_2 in TA-CP and TA-HT can absorb hydrogen molecules and be partially reduced. Furthermore, metal species supported on the TA-CP and TA-HT are more easily reduced and better dispersed. For the NiMoP catalysts prepared with TA-CP and TA-HT, the Ti element promotes the sulfidation degree of Mo, besides shortening the average (Ni)MoS_2 slab. The catalysts prepared with TA-CP exhibited superior activity for 4,6-DMDBT hydrodesulfurization. This can be ascribed not only to the relatively high sulfidation degree of Mo and proportion of the NiMoS active phase but also to the well-dispersed (Ni)MoS_2 slabs. Moreover, the Ti^{4+} ions dispersed in the Al_2O_3 skeleton can be partially reduced to act as electron donors, enhancing the metallic character of the S layers in MoS_2, which facilitates the improvement of the hydrogenation desulfurization activity.

Keywords: TiO_2-Al_2O_3 composite oxides; anatase; incorporation modes; reducible Ti species; hydrodesulfurization

check for updates

Citation: Hou, R.; Yang, Q.; Zeng, S.; Bao, J.; Nie, H.; Yang, C.; Jia, Y.; Hu, A.; Dai, Q. Optimizing the Incorporation Modes of TiO_2 in TiO_2-Al_2O_3 Composites for Enhancing Hydrodesulfurization Performance of Corresponding NiMoP-Supported Catalysts. *Catalysts* **2024**, *14*, 287. https://doi.org/10.3390/catal14050287

Academic Editor: Leonarda Liotta

Received: 28 March 2024
Revised: 18 April 2024
Accepted: 22 April 2024
Published: 24 April 2024

1. Introduction

With increasingly stringent environmental standards, the deep removal of sulfur components in crude oil poses a major challenge to the refining industry [1–4]. Hydrodesulfurization (HDS) is considered to be the most efficient process to remove these sulfur compounds [5], and the design and investigation of catalysts is a critical factor in improving HDS catalytic performance. Currently, the most widely utilized HDS catalysts are bulk catalysts and supported catalysts. Although bulk catalysts exhibit superior performance, their high metal content and high price restrict their application. From this point of view, supported HDS catalysts with relatively low metal content and better textural characteristics can be a more attractive option. Supported catalyst design and optimization involve various parameters, such as the pore structure of the support and the morphology of the active phase [6–9]. The superior pore structure enhances the diffusion of reactant and product molecules and facilitates the dispersion of active metals [10,11]. In addition, the support surface properties determine the metal–support interaction, which further contributes to the morphology of the active metal in sulfided hydrogenation catalysts [12–14].

γ-Al_2O_3 is frequently applied as an industrial hydrogenation catalyst support material for its low cost, relatively superior pore structure, excellent stability, and easy formation.

Nonetheless, environmental regulations require deep removal of organosulfur compounds such as 4,6-dimethylbenzothiophene (4,6-DMDBT), and the steric hindrance caused by methyl groups makes those compounds hard to remove; in some cases, it is difficult to meet the requirement for HDS catalyst capacity using pure γ-Al_2O_3 as a support [7,8]. Among other candidate support materials, researchers found that TiO_2-supported catalysts show higher HDS activity than γ-Al_2O_3-supported catalysts due to the presence of "chemical ligand effects" in titania [15–17]. However, the low thermal stability and low surface area of TiO_2 hinder its application as an industrial catalyst support. Thus, considerable efforts have been made to prepare high-performance composite support materials containing TiO_2, especially TiO_2-Al_2O_3 composites. Santes et al. [18] prepared three TiO_2-Al_2O_3 composites by different methods: impregnation, co-precipitation, and the sol–gel method. The TiO_2-Al_2O_3 composite prepared by the sol–gel method exhibited better pore distribution and higher pore volume, while the composite prepared by the co-precipitation approach had the largest surface area. For the TiO_2-Al_2O_3 composites prepared via the impregnation method, XRD patterns evidence the formation of anatase crystallites and verify a poor dispersion of TiO_2. Gasoil hydrotreating evaluations showed that the activity of the catalysts was improved by introducing TiO_2 into the γ-Al_2O_3 support. Huang et al. [19] prepared different Ti/Al molar ratios of TiO_2-Al_2O_3 binary oxides through a pre-hydrolysis co-precipitation procedure. As verified by the XRD patterns, there is almost no complete crystal phase of Al_2O_3 or TiO_2 in the supports with a Ti/Al molar ratio of 1 or 2. TiO_2-Al_2O_3 supports presented moderate metal–support interaction (MSI) and higher sulfidation degree of active metal. In addition, the quantity of coordinatively unsaturated sites (CUSs) increased with the introduction of Ti elements. The above-mentioned characteristics are conducive to improving the catalytic performance in the heavy oil hydrotreating process. Zhang et al. [20] synthesized highly ordered mesoporous TiO_2-Al_2O_3 composite oxides with different Ti/Al molar ratios using a facile self-assembly method triggered by evaporation. The highly ordered TiO_2-Al_2O_3 composites possess a highly specific area and narrow pore size distribution. It was demonstrated that the introduction of TiO_2 could weaken the MSI and favor the formation of the "Type II" Ni-Mo-S active phase. Furthermore, the NiMo catalyst with a Ti/Al molar ratio of 0.4 showed the highest 4,6-DMDBT HDS performance. Ferdous et al. [21] investigated the physicochemical properties of a series of NiMo catalysts supported on TiO_2-Al_2O_3. The introduction of titania contributed to improving the dispersion degree of active metal and facilitating the formation of polymolybdenum oxide on the catalysts. As a result, titania-modified Al_2O_3 could facilitate the HDS and hydrodenitrogenation (HDN) activities of catalysts. The study verified that introducing TiO_2 to Al_2O_3 can enhance the sulfidation degree of the active metal and the catalytic performance. Nevertheless, the present research has focused on evaluating the effects of introducing TiO_2 and variation in TiO_2 content on catalytic performance. The characteristics of TiO_2-Al_2O_3 synthesized by different methods varied, and the connection pattern of Ti and Al atoms is the main reason for this phenomenon, which has not been studied in detail. Therefore, the effect of incorporation modes and existence states of titania in TiO_2-Al_2O_3 on the properties of the catalytic materials and NiMoP catalyst performance was further investigated.

In this study, a series of TiO_2-Al_2O_3 composites were synthesized via co-precipitation, impregnation, and co-precipitation–hydrothermal methods. The pore structures of the four investigated supports are generally homogeneous, and appropriate characterization methods were used to determine the crystallinity and the variation in hydroxyl group intensity of samples. The reduction and the dispersion degree of Ti atoms were evaluated. The corresponding NiMoP-supported catalysts were characterized to investigate the coordination states of NiMo precursors and the variations of their interaction with TiO_2-Al_2O_3 supports. After sulfidation, the active phase morphologies and the covalent states of sulfided catalysts were examined. Finally, 4,6-dimethylbenzothiophene (4,6-DMDBT) was selected as a probe molecule to explore the influence of the incorporation modes of TiO_2 on the hydrodesulfurization performances of the corresponding catalysts.

2. Results and Discussion

2.1. Properties of the Synthesized Supports

The XRD patterns of the TiO_2-Al_2O_3 together with the Al_2O_3 supports were recorded, and the results are shown in Figure 1. As Figure 1 shows, all samples exhibited the diffraction peaks of γ-Al_2O_3 (2θ of about 36°, 45°, and 67°) (JCPDS card No. 10-0425). In addition, the diffraction peaks at about 25°, 48°, 54°, and 55° for the TA-I and TA-HT samples are identified as anatase (JCPDS card No. 21-1272). For TA-I, when the amount of the titania exceeded the largest capacity of the monolayer distribution on Al_2O_3, TiO_2 existed in the form of anatase by aggregation. The presence of XRD patterns of anatase indicates poor dispersion of TiO_2 in TiO_2-Al_2O_3 synthesized via the impregnation method, which is consistent with the results in the literature [18]. As shown in Figure 1, TA-CP did not show any anatase diffraction peaks; this result implied that the Ti atoms entered and were well dispersed in the Al_2O_3 skeleton during the co-precipitation process. However, after hydrothermal treatment, the Ti atoms dispersed in Al_2O_3 aggregated through hydroxyl linkage and showed anatase diffraction peaks. The XRD results for all TiO_2-containing supports demonstrated that the introduction of TiO_2 affects the intensity of the diffraction peaks of γ-Al_2O_3, indicating that the alumina particle size and crystallinity were changed.

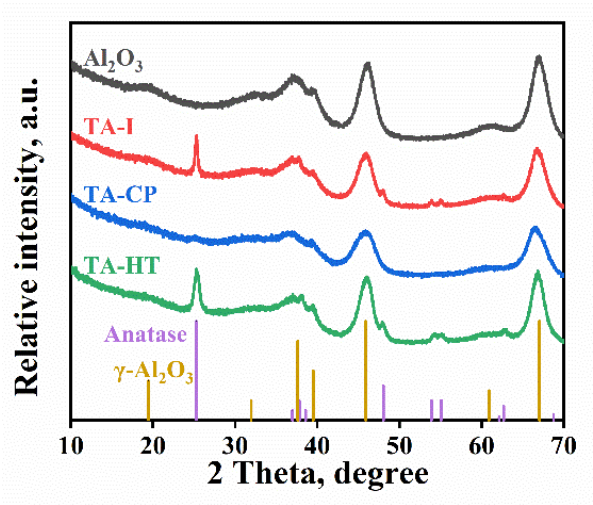

Figure 1. Wide-angle XRD results of the supports.

Figure 2 displays the pore diameter distributions of synthesized TiO_2-Al_2O_3 and Al_2O_3 supports, and Table 1 shows a summary of the pore structures of synthesized samples. The specific surface area, pore volume, and average pore size of TA-I and TA-CP supports were slightly reduced compared to those of Al_2O_3 support. The aggregation of TiO_2 on the composite support affects the textural parameters [19]. In the case of TA-I, the TiO_2 particles agglomerated on the surface of the Al_2O_3 support, which decreased the pore volume, surface area, and average pore diameter. Meanwhile, the pore volume and specific surface area of TA-HT were almost similar to those of the Al_2O_3 support. Moreover, for TA-HT, the average pore diameter was slightly larger than that of Al_2O_3 support.

Table 1. Textural properties of the supports.

Sample	S_{BET}, $m^2 \cdot g^{-1}$	V_p, $cm^3 \cdot g^{-1}$	D_{ave}, nm	Al_2O_3, wt%	TiO_2, wt%
Al_2O_3	240	0.68	8.47	100	0
TA-I	220	0.58	8.16	88.96	11.04
TA-CP	224	0.61	8.02	89.31	10.69
TA-HT	240	0.66	9.39	89.24	10.76

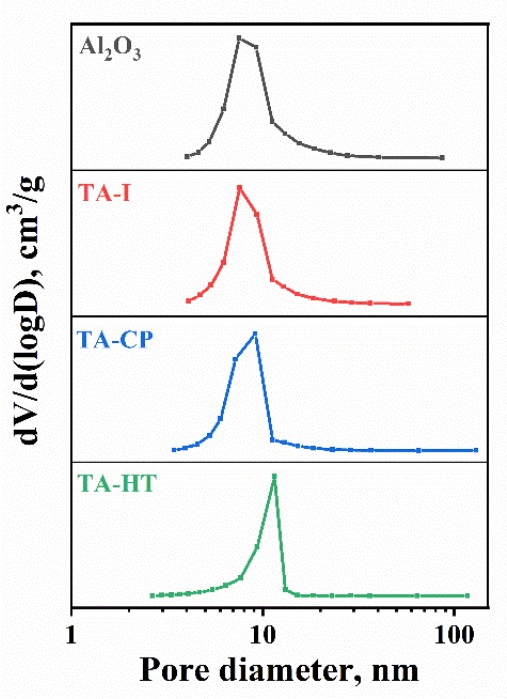

Figure 2. Pore size distribution of the supports.

Compared with TA-CP, the textural changes of TA-HT should be mainly attributed to the formation and growth of boehmite crystals during the hydrothermal treatment. As calculated by Scherrer's formula [22], the grain size of the boehmite particles increased from 3.3 nm to 6.2 nm after 150 °C for 4 h hydrothermal treatment. With the particle growth during hydrothermal treatment, TA-HT exhibited a higher average pore diameter and narrower pore distribution than TA-CP.

Figure 3 shows the FTIR spectra of TiO_2-Al_2O_3 support synthesized by various methods. The pure TiO_2 support exhibits a broad band around 450 cm^{-1} to 680 cm^{-1}, where the IR band at 495 cm^{-1} is assigned to the Ti-O-Ti bridge vibration of the anatase, and the bands between 550 and 653 cm^{-1} are attributed to the Ti-O vibrations [23]. The AlO_4 vibrations are responsible for the bands 700 and 900 cm^{-1}, while the AlO_6 stretching is responsible for the band at roughly 600 cm^{-1} [24,25]. There was overlapping of the characteristic vibrational intervals of TiO_2 and Al_2O_3 and a relatively small amount of titania, and no obvious Ti-O bonding vibrations were seen in the FTIR spectrum of supports. Characteristic vibrations of hetero metal–oxygen bonds of Ti-O-Al appear at 439 and 583 cm^{-1} [26]. Based on the spectral results, the intensity of the TA-I at 583 cm^{-1} was significantly higher than that of other samples, which indicates the presence of multiple Ti-O-Al bonds in TA-I. Therefore, when a TiO_2-Al_2O_3 support is synthesized through the impregnation method, TiO_2 and Al_2O_3 are preferentially connected through the surface hydroxyl groups.

Furthermore, Al_2O_3 and TA-I exhibited characteristic peaks at 1100 cm^{-1}, which could be ascribed to an Al-O bond. On the contrary, both TA-CP and TA-HT exhibited almost no variation at 1100 cm^{-1}, demonstrating that the presence of TiO_2 affects the Al-O bond when TiO_2-Al_2O_3 is synthesized by the co-precipitation method [27]. During the co-precipitation process, the Ti atom is proposed to be incorporated into the surface vacancy of Al_2O_3. According to the absence of any XRD characteristic peaks of TiO_2 in TA-CP, it can be concluded that the dispersion of TiO_2 in TA-CP is better with the same amount of TiO_2 doping. This phenomenon is consistent with the embedding model which has been proved in many works in the literature [28–30].

Given that the nature and amount of surface hydroxyl groups determine the dispersion of the metal species [31], we used IR spectroscopy to characterize the distribution of hydroxyl groups in the prepared supports, as illustrated in Figure 4. Generally, basic,

neutral, and acidic hydroxyl groups were identified with the bands located around 3772, 3726, and 3680 cm^{-1}, respectively [32]. Furthermore, for TiO_2-Al_2O_3 supports, the band centered around 3720 cm^{-1} can be regarded as the Ti-OH group [33].

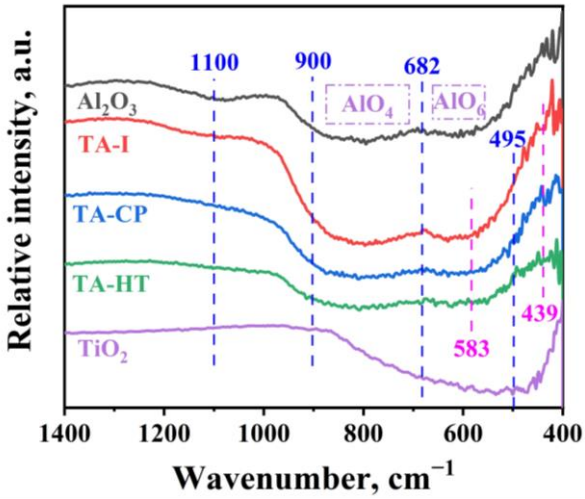

Figure 3. Skeletal FTIR spectra of TiO_2-Al_2O_3 support with various preparation methods.

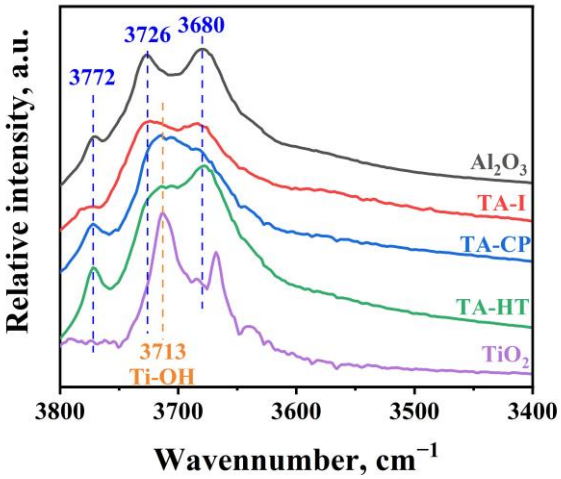

Figure 4. IR bands for synthesized supports in the 3400–3800 cm^{-1} spectra region.

The results in Figure 4 indicate that, compared with Al_2O_3 support, the number of total hydroxyl groups, especially the number of basic hydroxyl groups, in TA-I decreased, which is attributed to the TiO_2 connected with Al_2O_3 through the surface hydroxyl groups. According to previous research, the formation of the basic hydroxyl group is mainly caused by defects in the configuration of Al_2O_3 crystals [34]. Considering the FT-IR results and the increase in basic hydroxyl groups of TA-CP and TA-HT in combination, it can be stated that Ti atoms entered the surface vacancy and affected the lattice of alumina during the co-precipitation.

Moreover, the blue shift of the TA-CP and TA-HT neutral hydroxyl spectrum was due to the influence of the Ti-OH. Comparing the intensity of the hydroxyl group band at 3720 cm^{-1} for TA-CP and TA-HT supports, it can be found that the relative intensity of Ti-OH decreased after hydrothermal treatment. Based on the literature [35,36], when deionized water was used as the solvent, a high concentration of hydroxyl radicals was generated during the hydrothermal treatment, and hydroxyl radicals might interact with the surface titanium atoms. When the hydrothermal treatment temperature is above 100 °C, hydrogen bonds between chemisorbed water molecules and the lattice oxygen or adjacent OH^- groups recombine as dehydration occurs, transforming weaker hydrogen bonds into stronger bonds [37]. Combined with the decrease in the relative intensity of Ti-OH

compared to TA-CP, this result reveals that the hydroxyl groups that interacted with Ti atoms recombined and formed Ti-O-Ti during the hydrothermal treatment.

The titanium element distribution in the TiO_2-Al_2O_3 supports was verified using EPMA, and the results are shown in Figure 5. As Figure 5 manifests, the distribution of titanium elements in the alumina matrix is significantly influenced by the preparation methods. The dispersion degree of Ti elements in TiO_2-Al_2O_3 supports is increased in the order of TA-I < TA-HT < TA-CP.

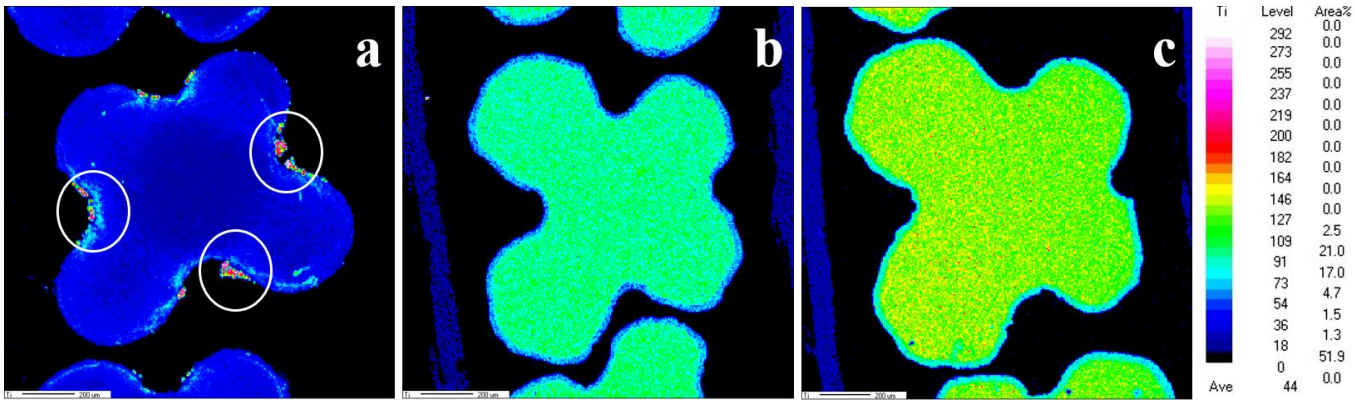

Figure 5. EPMA results for Ti elements in the TiO_2-Al_2O_3 supports: (**a**) TA-I, (**b**) TA-CP, (**c**) TA-HT.

As shown in Figure 5a, when the TiO_2-Al_2O_3 support was made by the impregnation method, Ti elements were more likely to aggregate on the alumina supports. Based on the previous characterization results, the TiO_2 in TA-I was connected to the Al_2O_3 through hydroxyl groups, but the number of hydroxyl groups of the Al_2O_3 was limited. As a result, the Ti elements in TA-I will aggregate and form anatase. Meanwhile, the Ti elements in TA-CP and TA-HT were more uniformly dispersed in the alumina skeleton, as shown in Figure 5b,c. Furthermore, the red dots that appear in Figure 5c suggest that Ti elements in TA-HT exhibited linkage during the hydrothermal treatment.

To identify the properties of various oxide specie present on the TiO_2-Al_2O_3 composites, H_2 temperature-programmed reduction (H_2-TPR) analysis was conducted, and the profiles are given in Figure 6. As can be observed in Figure 6, all synthesized supports show hydrogen reduction peaks between 450 and 700 °C, which can be partly attributed to the reduction of sulfate [38]. For TiO_2-containing supports, the H_2 consumption profile located at 430 °C is also associated with the reduction of anatase [39]. The low-temperature reduction peak temperatures of the synthesized support increase in the order of TiO_2 < TA-I < Al_2O_3 < TA-CP < TA-HT. For TiO_2-Al_2O_3 supports, the low-temperature reduction peaks were shifted towards higher temperatures; that phenomenon is associated with titania stabilization by interaction with the alumina [40]. Owing to the higher temperature of the low-temperature reduction peaks of TA-CP and TA-HT, we can conclude that the interaction between Al_2O_3 and TiO_2 is slightly stronger in the supports synthesized by the co-precipitation method.

During the heating process, anatase will undergo crystalline transformation to rutile at about 750 °C, and the rutile phase will appear at a reduction peak at T_{max} > 770 °C in the H_2-TPR profiles [41]. Compared with TA-I, TA-CP and TA-HT showed a more pronounced reduction peak located at T_{max} > 770 °C, indicating the presence of more reducible Ti species in these supports. Unlike the conventional profiles, when the reduction temperature was below 400 °C, the TCD signals of TA-CP and TA-HT both showed a decreasing trend. Considering this result in combination with the mechanism of H_2-TPR, it was presumed that Ti atoms dispersed in the alumina skeleton could absorb hydrogen molecules at low temperatures.

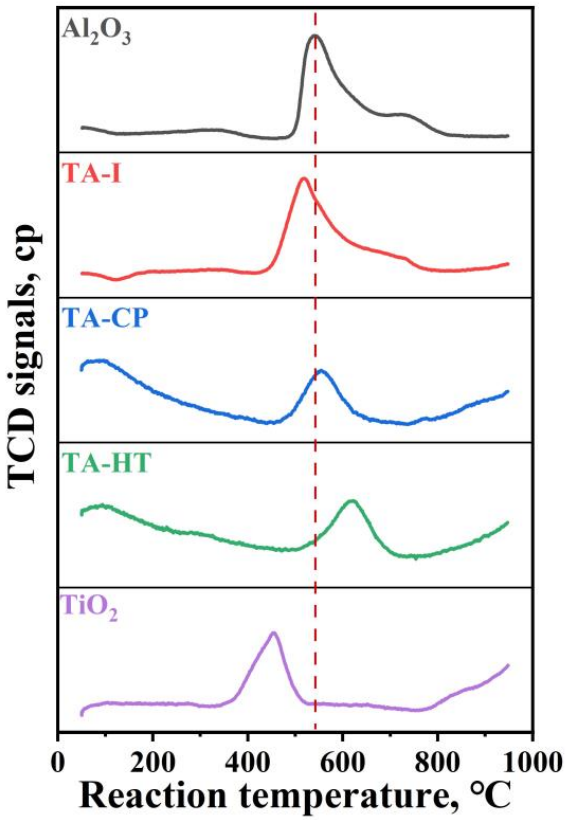

Figure 6. H_2-TPR profiles of the synthesized supports.

2.2. MSI of the Synthesized Catalysts

To further examine the effect of anatase incorporation in alumina on MSI, H_2-TPR characterization was employed, and the obtained profiles are exhibited in Figure 7. There are mainly three peaks: The peak located at around 300~400 °C is attributed to the reduction from Mo^{6+} to Mo^{4+}, and the peak centered at approximately 500 °C is assigned to the reduction of the Mo^{6+} species that strongly interacted with the TiO_2 to the lower coordinated species. The high-temperature reduction peak centered at around 800 °C is attributed to the reduction from Mo^{4+} to Mo^0 [8]. Besides that, the higher temperature peak between the 542 °C and 812 °C interval of CAT-T is also partly attributed to the reduction of the support material itself [42,43].

The position of the low-temperature reduction peak of CAT-T shifted to a higher temperature relative to CAT-A, indicating that the reduction of Mo^{6+} loaded on the reducible titania to Mo^{4+} was more difficult. The low-temperature reduction peaks of CAT-CP and CAT-HT were shifted to lower temperatures, demonstrating that TA-CP and TA-HT supports were conducive to Mo^{6+} reduction compared to Al_2O_3 and TA-I. Following the support TPR results, TA-CP and TA-HT will absorb hydrogen at low temperatures (<400 °C), a trait that promotes Mo^{6+} reduction. On the contrary, TA-I exhibited the opposite effect on the Mo^{6+} reduction process. Given the above, when titania is connected with alumina through hydroxyl groups, e.g., CAT-I, the reduction of active metals supported on TA-I is more difficult. The TPR peak centered at around 800 °C of TiO_2-containing catalysts, especially CAT-CP and CAT-HT, shifted to a higher temperature; this phenomenon demonstrates the SMSI, which is consistent with the relatively high intensity of the basic hydroxyl peaks [34] and the existence of Ti-OH of TA-CP and TA-HT supports. This SMSI also has been identified from the Raman results of Figure S1 in the Supplementary Materials. Moreover, CAT-CP and CAT-HT showed a shoulder peak of 400~600 °C, which can be attributed not only to the reduction of high coordinated Mo that interacted with TiO_2 but also to the presence of the Ti^{4+} reduction.

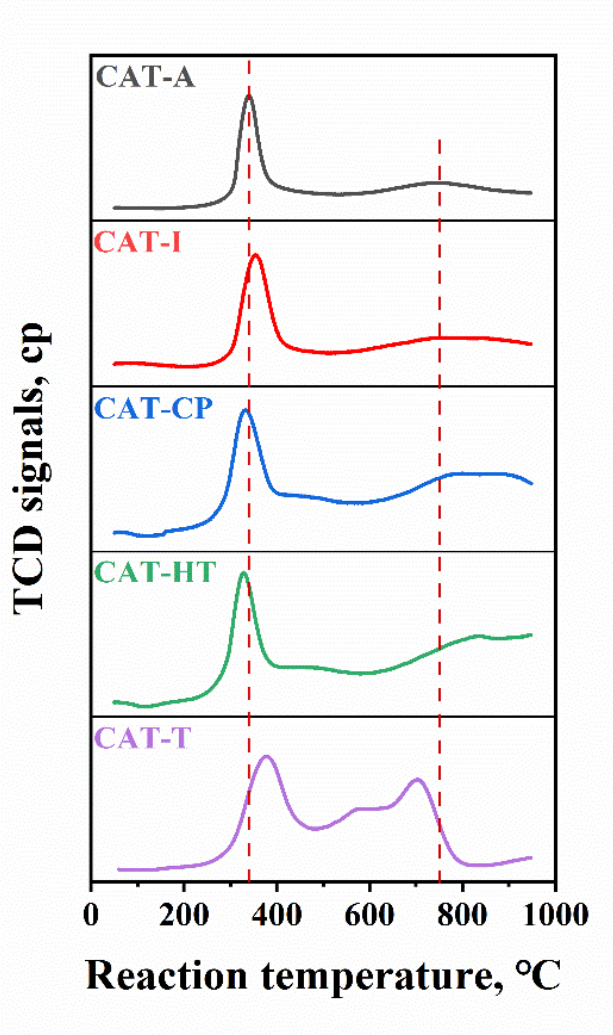

Figure 7. H_2-TPR profiles of the synthesized catalysts.

2.3. Morphologies of the Sulfided Catalysts

Representative HRTEM micrographs for further examination of the effect of TiO_2 modification on the morphology of the sulfided catalysts are displayed in Figure 8, and the statistical results are summarized in Table 2. The typical thread-like layers of (Ni)MoS_2 slabs could be seen in all the HRTEM images. Table 2 indicates that the degree of (Ni)MoS_2 slab stacking is not significantly affected by the introduction of TiO_2. In contrast, the length of the (Ni)MoS_2 slabs shortened following the incorporation of TiO_2. The average slab length of (Ni)MoS_2 increases in the following order: CAT-CP < CAT-HT < CAT-I < CAT-A. For TA-CP and TA-HT, both of which have more basic hydroxyl groups and Ti-OH, accordingly, the dispersion degree of Mo is higher, and the average (Ni)MoS_2 slab length of sulfided CAT-CP and CAT-HT is shorter. The higher dispersion degree of active metals on titania-containing supports is consistent with the Raman results of Figure S1 in the Supplementary Materials.

Table 2. Statistical details for average slab length, average stacking number, and D_{Mo} of (Ni) MoS_2.

Catalysts	CAT-A	CAT-I	CAT-CP	CAT-HT
Average slab length, nm	3.88	3.56	3.03	3.42
Average stacking number	1.6	1.6	1.4	1.7
D_{Mo}	0.26	0.27	0.33	0.29

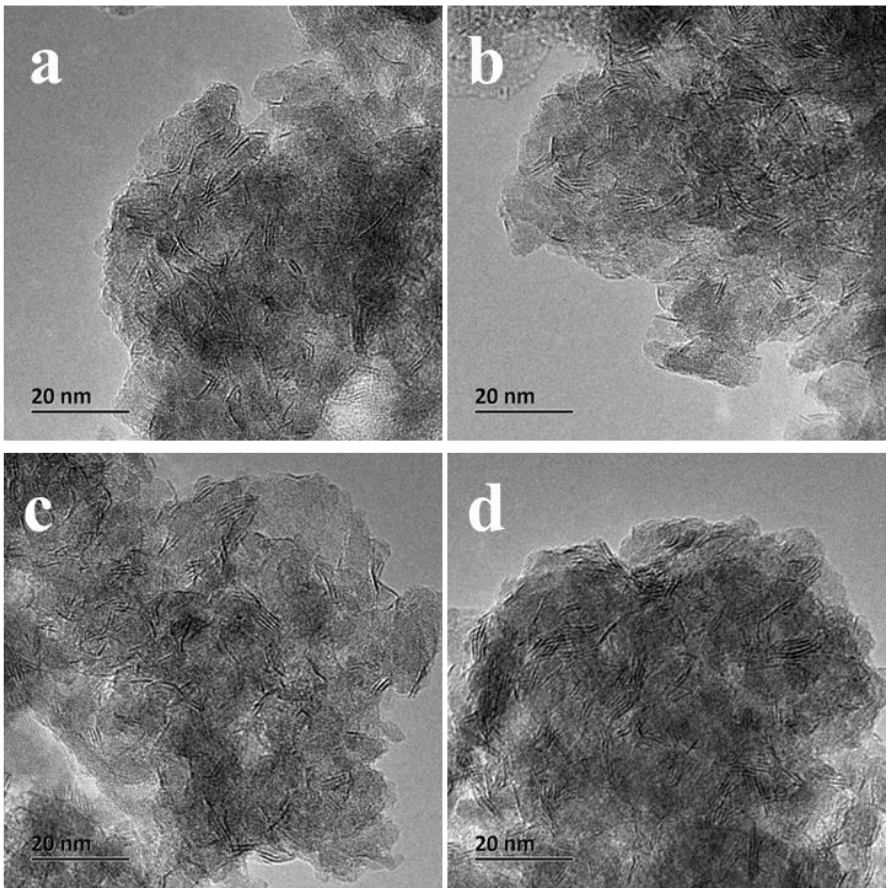

Figure 8. Representative HRTEM images of the sulfided catalysts: (**a**) CAT-A, (**b**) CAT-I, (**c**) CAT-CP, (**d**) CAT-HT.

2.4. Covalent States of the Sulfided Catalysts

X-ray photoelectron spectroscopy (XPS) was used to evaluate the effect of Ti species on the covalent states and sulfidation degrees of the active metals in the sulfided catalysts. Moreover, the deconvolution results according to the literature method [44–46] are shown in Figure 9a, and the calculated results are shown in Table 3. As observed in Figure 9a, the area of Mo^{5+} and Mo^{6+} peaks of CAT-CP and CAT-HT decreased notably, indicating that the sulfidation degree of Mo ($Mo_{sulfidation}$) was enhanced compared with CAT-A. On the contrary, the Mo^{5+} and Mo^{6+} peak areas of CAT-I increased relative to CAT-A, which can be explained by the results of H_2-TPR, where the low-temperature reduction peaks of CAT-CP and CAT-HT were shifted to a lower temperature. This feature makes it easier to reduce Mo^{6+} to Mo^{4+} during the sulfidation process. The reduction of Mo^{6+} to Mo^{4+} is difficult in CAT-I, and the sulfation degree of Mo is relatively lower. The calculated results are summarized in Table 3, and the $Mo_{sulfidation}$ increases according to the order of CAT-I < CAT-A < CAT-HT < CAT-CP.

The proportions of the NiMoS phase in the investigated catalysts were calculated based on Figure 9b, and the results are summarized in Table 3. Table 3 indicates that the proportion of the NiMoS phase in titania-containing catalysts is relatively higher. This phenomenon can be ascribed to the fact that the introduction of TiO_2 into Al_2O_3 prevents Ni from entering the alumina vacancies. Compared with CAT-I, the promotion of Ni is relatively weak on CAT-CP and CAT-HT. According to the available literature [47], MoS_2 supported on titania demonstrates mainly Mo edges, and this structure with fewer defective sites does not favor Ni promotion. Moreover, in comparison with CAT-CP and CAT-HT, after hydrothermal treatment, the Ti elements dispersed in the alumina skeleton showed anatase characteristic peaks through linkage and aggregation, and the proportion of the NiMoS phase was further reduced.

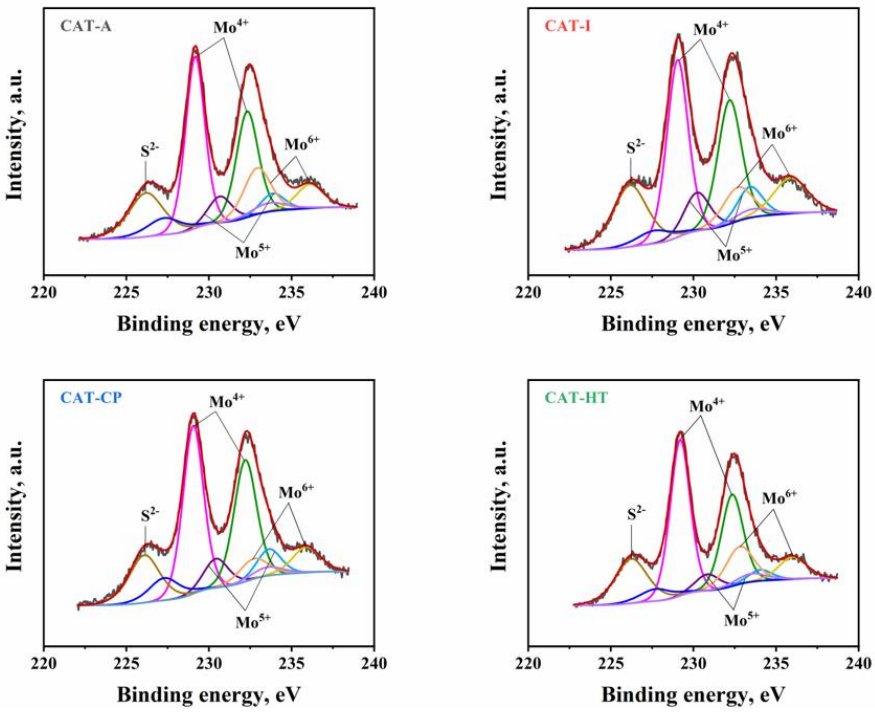

(**a**) Mo 3d

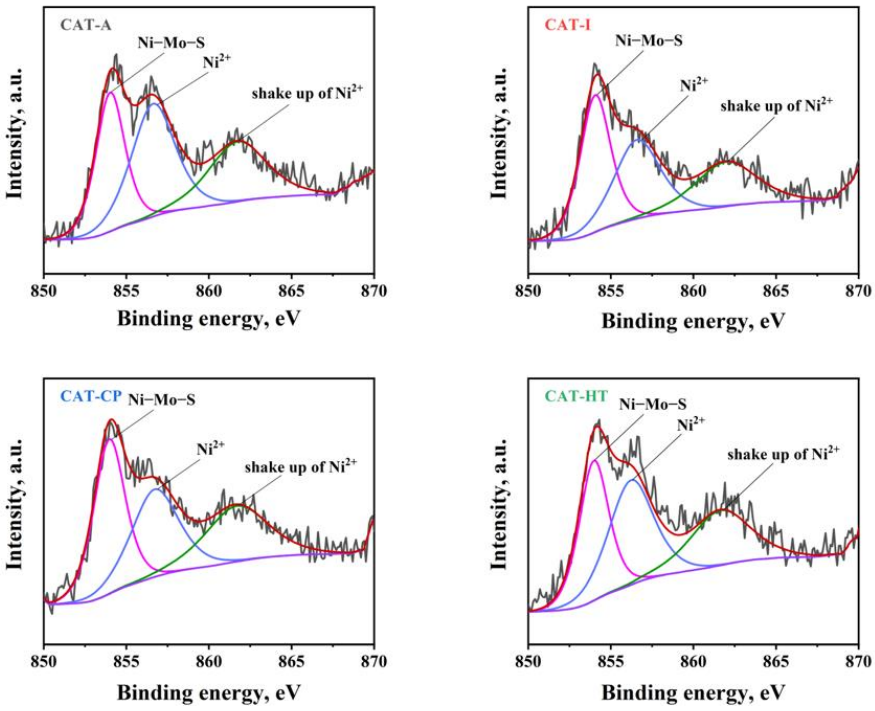

(**b**) Ni 2p

Figure 9. Deconvolution results for XPS of the sulfided catalysts.

Table 3. XPS calculated results of sulfided catalysts.

Samples	Sulfidation Degree of Mo, %	Proportion of NiMoS, %
CAT-A	65.68	32.46
CAT-I	62.75	39.77
CAT-CP	70.08	38.92
CAT-HT	68.89	34.39

2.5. Catalytic Performance Evaluation

In accordance with the above characterization results and analysis, it can be determined that the different forms of Ti elements in alumina will have different effects on the properties of the catalysts. To further analyze the influence of Ti elements on catalytic performance, 4,6-DMDBT was selected as the probe molecule, and the HDS test results over the sulfided catalysts at temperatures ranging from 260 °C to 300 °C are displayed in Figure 10. As Figure 10 shows, the total HDS activity (A_{total}) over the sulfided catalysts increased with increasing reaction temperatures. In addition, the A_{total} increases in a sequence of CAT-I < CAT-A < CAT-HT < CAT-CP at all investigated reaction temperatures.

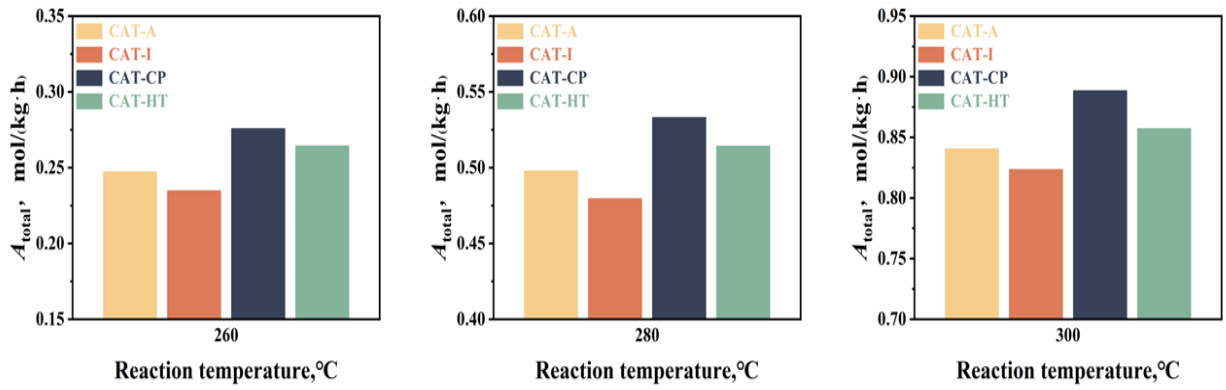

Figure 10. HDS of 4,6-DMDBT results of the synthesized catalysts.

According to previous research [20,48], the HDS of 4,6-DMDBT mainly proceeds through two parallel reaction pathways, as illustrated in Scheme 1. As shown in Scheme 1, 3,3′-dimethylbiphenyl (DM-BP) is formed through a direct desulfurization pathway (DDS), while the DM-BCH and DM-BCH are formed through a hydrogenation desulfurization. The steric hindrance posed by the presence of two methyl groups located at the 4 and 6 positions determines that the HYD route is the predominant reaction pathway during the 4,6-DMDBT HDS reaction.

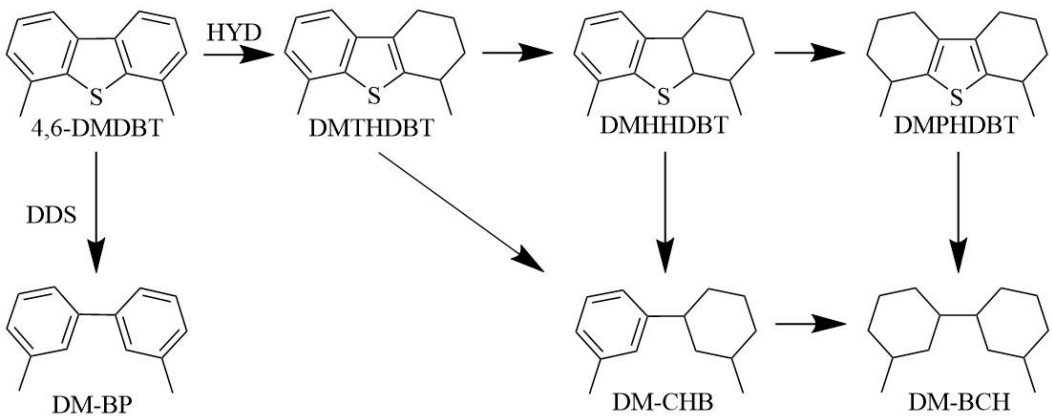

Scheme 1. The HDS reaction network for 4,6-DMDBT over synthesized catalysts.

To further investigate the HDS selectivity of 4,6-DMDBT, the A_{HYD} and A_{DDS} at reaction temperature 280 °C were calculated by Equations (2) and (3), and the results are noted in Table 4. Table 4 indicates that the A_{DDS} increased slightly after the addition of titania. In the meantime, the A_{HYD} of CAT-I decreased, whereas the A_{HYD} of CAT-CP and CAT-HT increased. For CAT-I and CAT-HT, the characteristic peaks of anatase have been detected; under the same A_{DDS}, the A_{HYD} of CAT-HT is relatively higher. Correspondingly, for CAT-CP, in which Ti is the most dispersed in the alumina skeleton, the A_{HYD} is the highest.

Table 4. Selectivity of 4,6-DMDBT HDS reaction over the sulfided catalysts at 280 °C.

Catalysts	CAT-A	CAT-I	CAT-CP	CAT-HT
A_{HYD} (mol·kg^{-1}·h^{-1})	0.45	0.42	0.48	0.46
A_{DDS} (mol·kg^{-1}·h^{-1})	0.05	0.06	0.06	0.06

Combined with the above characterization analysis of TiO_2-Al_2O_3 supports obtained by various preparation methods and corresponding synthesized catalysts, the following explanation is proposed for the differences in HDS results. When TiO_2-Al_2O_3 supports were synthesized by the co-precipitation method, Ti atoms were proposed to be incorporated into the surface vacancies of Al_2O_3. In this way, the reduction of Mo^{6+} loaded on the supports is promoted, which is conducive to increasing the sulfidation degree of Mo, e.g., CAT-CP (70.08%) and CAT-HT (68.89%). Moreover, with the relatively similar $Mo_{sulfidation}$ of CAT-CP and CAT-HT, the higher HDS activity of CAT-CP can be ascribed to the higher proportion of the NiMoS phase. Under hydrothermal treatment conditions, Ti atoms dispersed in alumina gradually connected and aggregated through Ti-OH, and the promotion of Ni on MoS_2 slabs was further weakened with the aggregation of TiO_2. But despite CAT-I having the highest NiMoS proportion of all catalysts, the activity is still low due to its lower $Mo_{sulfidation}$.

On the other hand, the intensity of basic hydroxyl groups on TA-CP and TA-HT supports are relatively higher, along with the appearance of a more pronounced characteristic peak of Ti-OH; these changes result in strong metal support interaction and increased Mo dispersion. This property makes the average (Ni)MoS_2 slab length of sulfided CAT-CP and CAT-HT relatively small; in particular, the (Ni)MoS_2 slab length of CAT-CP is significantly reduced. According to a previous literature study [49], for the same Mo atom loading, the larger (Ni)MoS_2 slabs imply fewer potential active sites. Therefore, the HDS activity of CAT-CP with a significantly short average (Ni)MoS_2 slab length (3.03 nm) was higher.

Furthermore, when Ti atoms are combined with Al_2O_3 via incorporation into surface vacancies and well dispersed in the Al_2O_3, Ti^{4+} ions in TA-CP and TA-HT can be partially reduced to Ti^{3+} ions under reduction conditions. The Ti^{3+} ions depict the existence of electronic density in both titania and molybdenum sulfide conduction bands. The delivery of electronic density between the titania and molybdenum sulfide causes the greater metallic character of the S layer in MoS_2 particles [47,50,51]. In the meantime, the greater metallic character of the MoS_2 presents higher hydrogenating capability. As a result, compared to the HYD activity of CAT-I (0.42), the CAT-CP (0.48) and CAT-HT (0.46) with reducible Ti species present higher HYD activity.

3. Materials and Methods

3.1. Materials

Raw materials: (1) aluminum sulfate ($Al_2(SO_4)_3$) solution, Al_2O_3: 104 g·L^{-1}; (2) sodium aluminate ($NaAlO_2$) solution, Al_2O_3: 220 g·L^{-1}, Na_2O: 227 g·L^{-1}; (3) titanium oxysulfate–sulfuric acid hydrate, Innochem (Beijing, China), synthesis grade; (4) titanium isopropoxide, Innochem (Beijing, China), 98%; (5) TiO_2, Saint-Gobain Norpro (Shanghai, China), ST61120; (6) molybdenum oxide, alkaline nickel carbonate, and phosphoric acid, Sinopharm Chemical Reagent Co., Ltd. (Beijing, China).

3.2. Synthesis of TiO_2-Al_2O_3 Composite Oxide Supports

Three different kinds of TiO_2-Al_2O_3 (10:90 wt%) supports were synthesized. The first one, named TA-I, was synthesized by the impregnation method. An appropriate amount of titanium isopropoxide was added to *n*-propanol to configure an impregnation solution, and then the impregnation solution was mixed with the butterfly-shaped extruded Al_2O_3 supports (SINOPEC Research Institute of Petroleum Processing Co., Ltd., Beijing, China) with a diameter of 1.6 mm via the pore volume impregnation method. After the

impregnation process, the modified samples were dried at 120 °C for 3 h and calcined at 550 °C for 3 h.

The other two TiO_2-Al_2O_3 composites were prepared by co-precipitation or hydrothermal methods and then molded to obtain the supports. In the procedure of preparing TiO_2-Al_2O_3 by co-precipitation, titanium oxysulfate–sulfuric acid hydrate was added to aluminum sulfate solution to form a homogeneous acidic solution with a concentration of 12.9 $g \cdot L^{-1}$ in terms of TiO_2 and 57.2 $g \cdot L^{-1}$ in terms of Al_2O_3. Then, the acid solution and the sodium aluminate solution were added to the tank simultaneously at a certain flow rate under vigorous stirring, and the pH of the reaction solution was controlled between 6.2 and 6.5. At the end of the co-precipitation session, sodium carbonate solution was added to the mixture to reach a pH between 8.9 and 9.2. Finally, the solution mixture was heated at 90 °C with stirring and aged for 6 h. The slurry was subsequently filtered and washed, and the cake was divided into two parts. One part was directly spray dried followed by extrusion into butterfly-shaped particles with a diameter of 1.6 mm and then dried in air at 120 °C for 3 h and calcined at 550 °C for 3 h, and the obtained support was recorded as TA-CP. The other part of the cake was redispersed in water and heated at 150 °C while being stirred in a hydrothermal autoclave. The resulting gel was washed with deionized water and dried and then extruded to obtain butterfly-shaped particles of 1.6 mm in diameter. Finally, the support, named TA-HT, was obtained by drying at 120 °C for 3 h and calcined at 550 °C for 3 h.

3.3. Preparation of NiMoP-Supported Catalysts

An incipient wetness co-impregnation method was used to prepare the corresponding NiMoP catalysts. A mixture of a solution containing molybdenum oxide, alkaline nickel carbonate, and phosphoric acid was used as the impregnation solution. The wet catalysts were first dried at 120 °C for 3 h and then calcined at 400 °C for 3 h. The catalysts possessed the same loading of 14.5 wt% MoO_3, 3.5 wt% NiO, and 3.0 wt% P_2O_5. The obtained catalysts were denoted as CAT-I, CAT-CP, and CAT-HT, respectively. When the support was pure Al_2O_3 or TiO_2, the corresponding catalyst was denoted as CAT-A or CAT-T.

3.4. Characterization of the Materials

The crystalline structure of the prepared samples was determined by wide-angle powder X-ray diffraction (XRD). The characterization was carried out on a Philips (Andover, MA, USA) XPERT advanced powder diffractometer with Cu Kα radiation (40 kV, 30 mA).

The pore structure of each support was characterized through nitrogen adsorption–desorption measurements at −196 °C on a Micromeritics (Norcross, GA, USA) ASAP 2420 analyzer. The samples were outgassed at 350 °C for 10 h while under vacuum before measurement.

The formation of interaction bands and the presence of hydroxyl groups in the range of 4000–400 cm^{-1} were assessed using Fourier-transform infrared spectroscopy (FT-IR) on a Nicolet (Green Bay, WI, USA) 870 Fourier-transform infrared spectrometer.

The elemental distribution of titanium and aluminum in the TiO_2-Al_2O_3 composites was examined by a JXA-8230 electron probe microanalyzer (EPMA) (Tokyo, Japan). The analyses were executed at a 15 kV accelerating voltage.

H_2 temperature-programmed reduction (H_2-TPR) of synthesized samples was performed to characterize the MSI on an AutoChemII2920 apparatus (Norcross, GA, USA). The flow rate was 10% H_2/Ar (by volume) at 50 $cm^3 \cdot min^{-1}$, and the temperature was raised to 950 °C at a rate of 10 $°C \cdot min^{-1}$, with a cold trap to condense the water vapor.

The Fourier-transformed Raman (FT-Raman) spectra for these catalysts were noted on a LabRAM (St. Petersburg, FL, USA) HR UV-NIR Raman apparatus equipped with a He-Cd laser (325 nm) to determine the NiMo precursor coordination states on the binary oxide surface.

High-resolution transmission electron microscopy (HRTEM) images of sulfided catalysts were recorded on a Tecnai G2 F20 S-TWIN microscope (Hillsboro, OR, USA). Before

the characterization, catalyst samples with a mesh size of 40–60 were sulfided utilizing the sulfidation method in a fixed-bed micro-reactor with 5 wt% CS_2 cyclohexane solution. The sulfidation procedure was performed at a temperature of 230 °C for one hour, and then at 360 °C for two hours, with a total pressure of 4.0 MPa, a liquid flow rate of 0.4 mL·min^{-1}, and a H_2 flow rate of 365 mL·min^{-1}. The sulfided catalysts were carefully unloaded and then put into cyclohexane to prevent oxidation. Each sample was captured in at least 20 micrographs, The (Ni)MoS slab morphology data for each sample were obtained by counting at least 800 slabs. The morphological details of the (Ni)MoS slab were statistically calculated as described in Section S1 in the Supplementary Materials.

X-ray photoelectron spectroscopy (XPS) was employed to determine the coordination states of the active metals on the sulfided catalysts. The XPS analysis was performed on a Thermo Fischer (Waltham, MA, USA)-VG ESCALAB 250 spectrometer using Al Kα radiation.

3.5. Catalytic Performance Assessment

The catalytic performance of the synthesized catalysts was determined using 4,6-DMDBT as the reactant and assessed on a continuous-flow fixed-bed micro-reactor with an inner diameter of 8 mm. And the sulfidation procedure and catalytic performance assessment method were described in the HRTEM characterization.

Then, the 4,6-DMDBT (0.45 wt% in decane) HDS reaction was performed at temperatures ranging from 260 °C to 300 °C. Decahydronaphthalene was added as an internal standard. The other test conditions were as follows: the liquid flow rate was 0.2 mL·min^{-1}, the total pressure was 4.0 MPa, and the H_2/oil volume ratio was 500. Following stabilization for 2 h, the liquid products were gathered and subjected to an offline analysis using an Agilent (Santa Clara, CA, USA) 7890A Gas Chromatograph equipped with a 30 m capillary column of HP-15 methyl siloxane and a flame ionization detector (FID).

There are two main mechanisms for the HDS reaction; one involves the substitution of a hydrogen atom for a sulfur atom in the hydrocarbon structure, defined as the direct desulfurization pathway (DDS), and the other includes the hydrogenation of the benzene ring followed by removal of the S atom, which is defined as hydrogenation desulfurization (HYD) [48]. As is verified, 4,6-THDMDBT, 4,6-HHDMDBT, 4,6-DM-PHDBT, 3,3′-DM-CHB, and 3,3′-DM-BCH are obtained by the HYD pathway, while 3,3′-DMBP is obtained by the DDS pathway [14]. The activity of 4,6-DMDBT HDS reaction over the prepared catalysts was calculated in the range of 260–300 °C according to the following equations [52]:

$$A_T = F_0 \times \frac{x}{m} \tag{1}$$

$$A_{DDS} = A_T \times S_{DDS} \tag{2}$$

$$A_{HYD} = A_T \times S_{HYD} \tag{3}$$

In Equations (1)–(3), F_0 stands for the molar flow rate of 4,6-DMDBT in mol·h^{-1}, x stands for the 4,6-DMDBT conversion, and m stands for the catalyst mass in kg. S_{DDS} is the selectivity of the DDS route, and S_{HYD} is the selectivity of the HYD route.

4. Conclusions

Titania–alumina composite oxides with a TiO_2 mass ratio of 10% were prepared by an impregnation method, co-precipitation method, and co-precipitation–hydrothermal treatment method. The effect of incorporation modes on the properties of TiO_2-Al_2O_3 supports and the HDS performance of NiMoP catalysts was investigated. Based on the characterization of supports and corresponding catalysts, we concluded that TiO_2 and Al_2O_3 are connected via surface hydroxyl groups in TA-I, whereas Ti atoms can be dispersed in the alumina skeleton and affect the nature of Al-O in TA-CP and TA-HT. In addition, Ti atoms dispersed in the alumina skeleton can promote the reduction of Mo^{6+} to Mo^{4+} and further increase the sulfidation degree of Mo. For TA-CP and TA-HT, the increase in the

intensity of basic hydroxyl and titanium hydroxyl groups is conducive to the dispersion of the active metal on supports and shortens the average Ni-promoted MoS_2 slab length. Depending on the higher dispersion degree of Ti atoms in TA-CP, the titanium hydroxyl group intensity is higher; consequently, the average length of (Ni)MoS_2 slabs in the sulfided catalyst is shorter. Moreover, TiO_2 in CAT-CP and CAT-HT can be partially reduced to Ti^{3+}, which makes MoS_2 more metallic due to its unique electronic effect.

Afterward, the HDS reaction of 4,6-DMDBT assessed the corresponding catalysts' activity. Optimal HDS activity of 4,6-DMDBT was obtained over CAT-CP, which was mainly attributed to the well-dispersed Ti atoms in the alumina skeleton not only improving the dispersion of the active metal but also increasing the Mo sulfidation degree and the proportion of NiMoS. In addition, the reducible TiO_2 also changed the morphology of MoS_2 slabs and enhanced HYD activity. This study presents ideas for synthesizing TiO_2-Al_2O_3 supports with high HDS performance.

Supplementary Materials: The following supporting information can be downloaded at: https://www.mdpi.com/article/10.3390/catal14050287/s1, Section S1 Statistical calculation methods of HRTEM, Figure S1: Raman spectra of the synthesized catalysts. Figure S2: Wide-angle XRD patterns of the synthesized catalysts. Refs. [51,53–61] are cited in Supplementary Materials.

Author Contributions: Conceptualization, R.H. and S.Z.; formal analysis, R.H. and S.Z.; investigation, R.H., S.Z. and J.B.; writing—original draft, R.H.; writing—review and editing, R.H., Q.Y., S.Z., J.B., H.N., C.Y., Y.J., A.H. and Q.D.; supervision, Q.Y. and H.N. All authors have read and agreed to the published version of the manuscript.

Funding: This work has been financially supported by a research grant from the National Key R&D Program of China (No. 2021YFA1501204) and the Project of SINOPEC (No. 123018).

Data Availability Statement: Data are contained within the article and Supplementary Materials.

Conflicts of Interest: The authors declare that this study received funding from SINOPEC Research Institute of Petroleum Processing Co., Ltd. The funder was not involved in the study design, collection, analysis, interpretation of data, the writing of this article or the decision to submit it for publication.

References

1. Xu, H.; He, P.; Li, Z.; Meng, S.; Li, Y.; Chang, L.-Y.; Liu, L.; Wen, X.; Klein, B.A.; Michaelis, V.K.; et al. Environmentally Benign Methane-Regulated Catalytic Desulfurization. *Appl. Catal. B Environ.* **2022**, *312*, 121436. [CrossRef]
2. Ali, I.; Saleh, T.A. Molybdenum Boron Based Catalysts Loaded on MnO Alumina Support for Hydrodesulfurization of Dibenzothiophene. *Inorg. Chem. Commun.* **2022**, *138*, 109237. [CrossRef]
3. Shi, Y.; Wang, G.; Mei, J.; Xiao, C.; Hu, D.; Wang, A.; Song, Y.; Ni, Y.; Jiang, G.; Duan, A. The Influence of Pore Structure and Acidity on the Hydrodesulfurization of Dibenzothiophene over NiMo-Supported Catalysts. *ACS Omega* **2020**, *5*, 15576–15585. [CrossRef]
4. Saleh, T.A. Global Trends in Technologies and Nanomaterials for Removal of Sulfur Organic Compounds: Clean Energy and Green Environment. *J. Mol. Liq.* **2022**, *359*, 119340. [CrossRef]
5. Jiang, B.; Zhu, T.; Song, H.; Li, F. Hydrodeoxygenation and Hydrodesulfurization over Fe Promoted Ni2P/SBA-15 Catalyst. *J. Alloys Compd.* **2019**, *806*, 254–262. [CrossRef]
6. Nikulshin, P.A.; Ishutenko, D.I.; Mozhaev, A.A.; Maslakov, K.I.; Pimerzin, A.A. Effects of Composition and Morphology of Active Phase of CoMo/Al_2O_3 Catalysts Prepared Using Co_2Mo_{10}–Heteropolyacid and Chelating Agents on Their Catalytic Properties in HDS and HYD Reactions. *J. Catal.* **2014**, *312*, 152–169. [CrossRef]
7. Zhou, W.; Zhou, A.; Zhang, Y.; Zhang, C.; Chen, Z.; Liu, L.; Zhou, Y.; Wei, Q.; Tao, X. Hydrodesulfurization of 4,6-Dimethyldibenzothiophene over NiMo Supported on Ga-Modified Y Zeolites Catalysts. *J. Catal.* **2019**, *374*, 345–359. [CrossRef]
8. Zhou, W.; Yang, L.; Liu, L.; Chen, Z.; Zhou, A.; Zhang, Y.; He, X.; Shi, F.; Zhao, Z. Synthesis of Novel NiMo Catalysts Supported on Highly Ordered TiO_2-Al_2O_3 Composites and Their Superior Catalytic Performance for 4,6-Dimethyldibenzothiophene Hydrodesulfurization. *Appl. Catal. B Environ.* **2020**, *268*, 118428. [CrossRef]
9. Topsøe, H.; Clausen, B.S. Importance of Co-Mo-S Type Structures in Hydrodesulfurization. *Catal. Rev.* **1984**, *26*, 395–420. [CrossRef]
10. Badoga, S.; Sharma, R.V.; Dalai, A.K.; Adjaye, J. Synthesis and Characterization of Mesoporous Aluminas with Different Pore Sizes: Application in NiMo Supported Catalyst for Hydrotreating of Heavy Gas Oil. *Appl. Catal. A Gen.* **2015**, *489*, 86–97. [CrossRef]

11. Zhang, D.; Liu, X.M.; Liu, Y.X.; Yan, Z.F. Impact of γ-Alumina Pore Structure on Structure and Performance of Ni–Mo/γ-Al_2O_3 Catalyst for 4,6-Dimethyldibenzothiophene Desulfurization. *Microporous Mesoporous Mater.* **2021**, *310*, 110637. [CrossRef]
12. Xia, B.; Cao, L.; Luo, K.; Zhao, L.; Wang, X.; Gao, J.; Xu, C. Effects of the Active Phase of CoMo/γ-Al_2O_3 Catalysts Modified Using Cerium and Phosphorus on the HDS Performance for FCC Gasoline. *Energy Fuels* **2019**, *33*, 4462–4473. [CrossRef]
13. López-Benítez, A.; Berhault, G.; Guevara-Lara, A. NiMo Catalysts Supported on Mn-Al_2O_3 for Dibenzothiophene Hydrodesulfurization Application. *Appl. Catal. B Environ.* **2017**, *213*, 28–41. [CrossRef]
14. Li, X.; Chai, Y.; Liu, B.; Liu, H.; Li, J.; Zhao, R.; Liu, C. Hydrodesulfurization of 4,6-Dimethyldibenzothiophene over CoMo Catalysts Supported on γ-Alumina with Different Morphology. *Ind. Eng. Chem. Res.* **2014**, *53*, 9665–9673. [CrossRef]
15. Naboulsi, I.; Lebeau, B.; Aponte, C.F.L.; Brunet, S.; Mallet, M.; Michelin, L.; Bonne, M.; Carteret, C.; Blin, J.-L. Selective Direct Desulfurization Way (DDS) with CoMoS Supported over Mesostructured Titania for the Deep Hydrodesulfurization of 4,6-Dimethydibenzothiophene. *Appl. Catal. A Gen.* **2018**, *563*, 91–97. [CrossRef]
16. Roy, T.; Rousseau, J.; Daudin, A.; Pirngruber, G.; Lebeau, B.; Blin, J.-L.; Brunet, S. Deep Hydrodesulfurization of 4,6-Dimethydibenzothiophene over CoMoS/TiO_2 Catalysts: Impact of the TiO_2 Treatment. *Catal. Today* **2021**, *377*, 17–25. [CrossRef]
17. Arrouvel, C.; Breysse, M.; Toulhoat, H.; Raybaud, P. A Density Functional Theory Comparison of Anatase (TiO_2)- and γ-Al_2O_3-Supported MoS_2 Catalysts. *J. Catal.* **2005**, *232*, 161–178. [CrossRef]
18. Santes, V.; Herbert, J.; Cortez, M.T.; Zárate, R.; Díaz, L.; Swamy, P.N.; Aouine, M.; Vrinat, M. Catalytic Hydrotreating of Heavy Gasoil FCC Feed on Alumina–Titania-Supported NiMo Catalysts. *Appl. Catal. A Gen.* **2005**, *281*, 121–128. [CrossRef]
19. Huang, W.; Zhou, Y.; Wei, Q.; Liu, X.; Zhang, P.; Xu, Z.; Yu, Z.; Wang, X.; Liu, H.; Dai, X.; et al. Synthesis of Mesoporous TiO_2-Al_2O_3 Composites Supported NiW Hydrotreating Catalysts and Their Superior Catalytic Performance for Heavy Oil Hydrodenitrogenation. *Fuel* **2022**, *319*, 123802. [CrossRef]
20. Zhang, P.; Mu, F.; Zhou, Y.; Long, Y.; Wei, Q.; Liu, X.; You, Q.; Shan, Y.; Zhou, W. Synthesis of Highly Ordered TiO_2-Al_2O_3 and Catalytic Performance of Its Supported NiMo for HDS of 4, 6-Dimethyldibenzothiophene. *Catal. Today* **2020**, *423*, 112716. [CrossRef]
21. Ferdous, D.; Bakhshi, N.N.; Dalai, A.K.; Adjaye, J. Synthesis, Characterization and Performance of NiMo Catalysts Supported on Titania Modified Alumina for the Hydroprocessing of Different Gas Oils Derived from Athabasca Bitumen. *Appl. Catal. B Environ.* **2007**, *72*, 118–128. [CrossRef]
22. Thompson, P.; Cox, D.E.; Hastings, J.B. Rietveld Refinement of Debye–Scherrer Synchrotron X-Ray Data from Al_2O_3. *J. Appl. Crystallogr.* **1987**, *20*, 79–83. [CrossRef]
23. Bezrodna, T.; Puchkovska, G.; Shymanovska, V.; Baran, J.; Ratajczak, H. IR-Analysis of H-Bonded H_2O on the Pure TiO_2 Surface. *J. Mol. Struct.* **2004**, *700*, 175–181. [CrossRef]
24. Song, H.; Dai, M.; Guo, Y.-T.; Zhang, Y.-J. Preparation of Composite TiO_2–Al_2O_3 Supported Nickel Phosphide Hydrotreating Catalysts and Catalytic Activity for Hydrodesulfurization of Dibenzothiophene. *Fuel Process. Technol.* **2012**, *96*, 228–236. [CrossRef]
25. Tarte, P. Infra-Red Spectra of Inorganic Aluminates and Characteristic Vibrational Frequencies of AlO_4 Tetrahedra and AlO_6 Octahedra. *Spectrochim. Acta Part A Mol. Spectrosc.* **1967**, *23*, 2127–2143. [CrossRef]
26. Tursiloadi, S.; Imai, H.; Hirashima, H. Preparation and Characterization of Mesoporous Titania–Alumina Ceramic by Modified Sol–Gel Method. *J. Non-Cryst. Solids* **2004**, *350*, 271–276. [CrossRef]
27. Badoga, S.; Sharma, R.V.; Dalai, A.K.; Adjaye, J. Hydrotreating of Heavy Gas Oil on Mesoporous Mixed Metal Oxides (M–Al_2O_3, M = TiO_2, ZrO_2, SnO_2) Supported NiMo Catalysts: Influence of Surface Acidity. *Ind. Eng. Chem. Res.* **2014**, *53*, 18729–18739. [CrossRef]
28. Khaleel, A. Titanium-Doped Alumina for Catalytic Dehydration of Methanol to Dimethyl Ether at Relatively Low Temperatures. *Fuel* **2011**, *90*, 2422–2427. [CrossRef]
29. Wang, J.; Dong, L.; Hu, Y.; Zheng, G.; Hu, Z.; Chen, Y. Dispersion of NiO Supported on γ-Al_2O_3 and TiO_2/γ-Al_2O_3 Supports. *J. Solid State Chem.* **2001**, *157*, 274–282. [CrossRef]
30. Yang, M.; Men, Y.; Li, S.; Chen, G. Enhancement of Catalytic Activity over TiO_2-Modified Al_2O_3 and ZnO–Cr_2O_3 Composite Catalyst for Hydrogen Production via Dimethyl Ether Steam Reforming. *Appl. Catal. A Gen.* **2012**, *433–434*, 26–34. [CrossRef]
31. Li, M.; Li, H.; Jiang, F.; Chu, Y.; Nie, H. Effect of Surface Characteristics of Different Alumina on Metal–Support Interaction and Hydrodesulfurization Activity. *Fuel* **2009**, *88*, 1281–1285. [CrossRef]
32. Morterra, C.; Magnacca, G. A Case Study: Surface Chemistry and Surface Structure of Catalytic Aluminas, as Studied by Vibrational Spectroscopy of Adsorbed Species. *Catal. Today* **1996**, *27*, 497–532. [CrossRef]
33. José Velasco, M.; Rubio, F.; Rubio, J.; Oteo, J.L. DSC and FT-IR Analysis of the Drying Process of Titanium Alkoxide Derived Precipitates. *Thermochim. Acta* **1999**, *326*, 91–97. [CrossRef]
34. Li, H.; Li, M.; Nie, H. Tailoring the Surface Characteristic of Alumina for Preparation of Highly Active NiMo/Al_2O_3 Hydrodesulfurization Catalyst. *Microporous Mesoporous Mater.* **2014**, *188*, 30–36. [CrossRef]
35. Etacheri, V.; Seery, M.K.; Hinder, S.J.; Pillai, S.C. Oxygen Rich Titania: A Dopant Free, High Temperature Stable, and Visible-Light Active Anatase Photocatalyst. *Adv. Funct. Mater.* **2011**, *21*, 3744–3752. [CrossRef]
36. Kusior, A.; Banas, J.; Trenczek-Zajac, A.; Zubrzycka, P.; Micek-Ilnicka, A.; Radecka, M. Structural Properties of TiO_2 Nanomaterials. *J. Mol. Struct.* **2018**, *1157*, 327–336. [CrossRef]

37. Li, G.; Li, L.; Boerio-Goates, J.; Woodfield, B.F. High Purity Anatase TiO_2 Nanocrystals: Near Room-Temperature Synthesis, Grain Growth Kinetics, and Surface Hydration Chemistry. *J. Am. Chem. Soc.* **2005**, *127*, 8659–8666. [CrossRef] [PubMed]
38. Jung, S.M.; Grange, P. Characterization and Reactivity of V_2O_5-WO_3 Supported on TiO_2-SO_4^{2-} Catalyst for the SCR Reaction. *Appl. Catal. B Environ.* **2001**, *32*, 123–131. [CrossRef]
39. Figueiredo, F.C.A.; Jordão, E.; Carvalho, W.A. Adipic Ester Hydrogenation Catalyzed by Platinum Supported in Alumina, Titania and Pillared Clays. *Appl. Catal. A Gen.* **2008**, *351*, 259–266. [CrossRef]
40. Núñez, S.; Escobar, J.; Vázquez, A.; Reyes, J.A.D.L.; Hernández-Barrera, M. 4,6-Dimethyl-Dibenzothiophene Conversion over Al_2O_3–TiO_2-Supported Noble Metal Catalysts. *Mater. Chem. Phys.* **2011**, *126*, 237–247. [CrossRef]
41. Ramírez, J.; Gutiérrez-Alejandre, A. Characterization and Hydrodesulfurization Activity of W-Based Catalysts Supported on Al_2O_3–TiO_2 Mixed Oxides. *J. Catal.* **1997**, *170*, 108–122. [CrossRef]
42. Karatzas, X.; Jansson, K.; González, A.; Dawody, J.; Pettersson, L.J. Autothermal Reforming of Low-Sulfur Diesel over Bimetallic RhPt Supported on Al_2O_3, CeO_2–ZrO_2, SiO_2 and TiO_2. *Appl. Catal. B Environ.* **2011**, *106*, 476–487. [CrossRef]
43. Liu, X.; Chen, H.; Wu, X.; Cao, L.; Jiang, P.; Yu, Q.; Ma, Y. Effects of SiO_2 Modification on the Hydrothermal Stability of the V_2O_5/WO_3–TiO_2 NH_3-SCR Catalyst: TiO_2 Structure and Vanadia Species. *Catal. Sci. Technol.* **2019**, *9*, 3711–3720. [CrossRef]
44. Galtayries, A.; Wisniewski, S.; Grimblot, J. Formation of Thin Oxide and Sulphide Films on Polycrystalline Molybdenum Foils: Characterization by XPS and Surface Potential Variations. *J. Electron. Spectrosc. Relat. Phenom.* **1997**, *87*, 31–44. [CrossRef]
45. Lai, W.; Song, W.; Pang, L.; Wu, Z.; Zheng, N.; Li, J.; Zheng, J.; Yi, X.; Fang, W. The Effect of Starch Addition on Combustion Synthesis of NiMo–Al_2O_3 Catalysts for Hydrodesulfurization. *J. Catal.* **2013**, *303*, 80–91. [CrossRef]
46. Zhou, W.; Liu, M.; Zhang, Q.; Wei, Q.; Ding, S.; Zhou, Y. Synthesis of NiMo Catalysts Supported on Gallium-Containing Mesoporous Y Zeolites with Different Gallium Contents and Their High Activities in the Hydrodesulfurization of 4,6-Dimethyldibenzothiophene. *ACS Catal.* **2017**, *7*, 7665–7679. [CrossRef]
47. Castillo-Villalón, P.; Ramírez, J.; Cuevas, R.; Vázquez, P.; Castañeda, R. Influence of the Support on the Catalytic Performance of Mo, CoMo, and NiMo Catalysts Supported on Al_2O_3 and TiO_2 during the HDS of Thiophene, Dibenzothiophene, or 4,6-Dimethyldibenzothiophene. *Catal. Today* **2016**, *259*, 140–149. [CrossRef]
48. García-Martínez, J.C.; Castillo-Araiza, C.O.; De Los Reyes Heredia, J.A.; Trejo, E.; Montesinos, A. Kinetics of HDS and of the Inhibitory Effect of Quinoline on HDS of 4,6-DMDBT over a Ni–Mo–P/Al_2O_3 Catalyst: Part I. *Chem. Eng. J.* **2012**, *210*, 53–62. [CrossRef]
49. Li, M.; Li, H.; Jiang, F.; Chu, Y.; Nie, H. The Relation between Morphology of (Co)MoS_2 Phases and Selective Hydrodesulfurization for CoMo Catalysts. *Catal. Today* **2010**, *149*, 35–39. [CrossRef]
50. Berger, T.; Sterrer, M.; Diwald, O.; Knözinger, E.; Panayotov, D.; Thompson, T.L.; Yates, J.T. Light-Induced Charge Separation in Anatase TiO_2 Particles. *J. Phys. Chem. B* **2005**, *109*, 6061–6068. [CrossRef]
51. Castillo-Villalón, P.; Ramírez, J. Spectroscopic Study of the Electronic Interactions in Ru/TiO_2 HDS Catalysts. *J. Catal.* **2009**, *268*, 39–48. [CrossRef]
52. Chen, W.; Maugé, F.; Van Gestel, J.; Nie, H.; Li, D.; Long, X. Effect of Modification of the Alumina Acidity on the Properties of Supported Mo and CoMo Sulfide Catalysts. *J. Catal.* **2013**, *304*, 47–62. [CrossRef]
53. Nikulshin, P.A.; Salnikov, V.A.; Mozhaev, A.V.; Minaev, P.P.; Kogan, V.M.; Pimerzin, A.A. Relationship between Active Phase Morphology and Catalytic Properties of the Carbon–Alumina-Supported Co(Ni)Mo Catalysts in HDS and HYD Reactions. *J. Catal.* **2014**, *309*, 386–396. [CrossRef]
54. Ninh, T.K.T.; Massin, L.; Laurenti, D.; Vrinat, M. A New Approach in the Evaluation of the Support Effect for NiMo Hydrodesulfurization Catalysts. *Appl. Catal. A Gen.* **2011**, *407*, 29–39. [CrossRef]
55. Badoga, S.; Mouli, K.C.; Soni, K.K.; Dalai, A.K.; Adjaye, J. Beneficial Influence of EDTA on the Structure and Catalytic Properties of Sulfided NiMo/SBA-15 Catalysts for Hydrotreating of Light Gas Oil. *Appl. Catal. B Environ.* **2012**, *125*, 67–84. [CrossRef]
56. Wang, X.; Zhao, Z.; Zheng, P.; Chen, Z.; Duan, A.; Xu, C.; Jiao, J.; Zhang, H.; Cao, Z.; Ge, B. Synthesis of NiMo Catalysts Supported on Mesoporous Al_2O_3 with Different Crystal Forms and Superior Catalytic Performance for the Hydrodesulfurization of Dibenzothiophene and 4,6-Dimethyldibenzothiophene. *J. Catal.* **2016**, *344*, 680–691. [CrossRef]
57. Muñoz-López, J.A.; Toledo, J.A.; Escobar, J.; López-Salinas, E. Preparation of Alumina–Titania Nanofibers by a pH-Swing Method. *Catal. Today* **2008**, *133–135*, 113–119. [CrossRef]
58. Obeso–Estrella, R.; Pawelec, B.; Mota, N.; Flores, L.; Melgoza, J.M.Q.; Yocupicio–Gaxiola, R.I.; Zepeda, T.A. Elucidating the Mechanisms of Titanium–Induced Morphological and Structural Changes in Catalysts on Mesoporous Al_2O_3–TiO_x Mixed Oxides: Effect of Non–Stoichiometric TiO_x Phase. *Microporous Mesoporous Mater.* **2022**, *339*, 111991. [CrossRef]
59. Vaiano, V.; Iervolino, G.; Sannino, D.; Rizzo, L.; Sarno, G.; Farina, A. Enhanced Photocatalytic Oxidation of Arsenite to Arsenate in Water Solutions by a New Catalyst Based on MoO_x Supported on TiO_2. *Appl. Catal. B Environ.* **2014**, *160–161*, 247–253. [CrossRef]
60. Dominguez Garcia, E.; Chen, J.; Oliviero, E.; Oliviero, L.; Maugé, F. New Insight into the Support Effect on HDS Catalysts: Evidence for the Role of Mo-Support Interaction on the MoS_2 Slab Morphology. *Appl. Catal. B Environ.* **2020**, *260*, 117975. [CrossRef]
61. Gao, D.; Duan, A.; Zhang, X.; Zhao, Z.; E, H.; Li, J.; Wang, H. Synthesis of NiMo Catalysts Supported on Mesoporous Al-SBA-15 with Different Morphologies and Their Catalytic Performance of DBT HDS. *Appl. Catal. B Environ.* **2015**, *165*, 269–284. [CrossRef]